Joint International Conference on Supercomputing in Nuclear Applications and Monte Carlo 2013 (SNA + MC 2013)
La Cité des Sciences et de l'Industrie, Paris, France, October 27–31, 2013

SAND2013-7609C

Evaluation of Monte Carlo Electron-Transport Algorithms in the Integrated Tiger Series Codes for Stochastic-Media Simulations

Brian C. Franke[1], Ronald P. Kensek[1], and Anil K. Prinja[2]

[1]*Sandia National Laboratories, P.O. Box 5800, MS 1179, Albuquerque, NM 87185 USA*
[2]*University of New Mexico, Department of Chemical and Nuclear Engineering, Albuquerque, NM 87131 USA*

Stochastic-media simulations require numerous boundary crossings. We consider two Monte Carlo electron transport approaches and evaluate accuracy with numerous material boundaries. In the condensed-history method, approximations are made based on infinite-medium solutions for multiple scattering over some track length. Typically, further approximations are employed for material-boundary crossings where infinite-medium solutions become invalid. We have previously explored an alternative "condensed transport" formulation, a Generalized Boltzmann-Fokker-Planck (GBFP) method, which requires no special boundary treatment but instead uses approximations to the electron-scattering cross sections. Some limited capabilities for analog transport and a GBFP method have been implemented in the Integrated Tiger Series (ITS) codes. Improvements have been made to the condensed history algorithm. The performance of the Integrated Tiger Series (ITS) condensed-history and condensed-transport algorithms are assessed for material-boundary crossings. These assessments are made both by introducing artificial material boundaries and by comparison to analog Monte Carlo simulations.

KEYWORDS: Electron Transport, Boundary Crossing, Stochastic Media, Condensed History

I. Introduction

Stochastic-media problems are generally characterized by frequent material-boundary crossings. Transport in such media can be problematic when the mean distance between boundaries is larger than the transport mean free path.[(1)] That is, the stochastic mixture can have an effect on the transport of electrons that cannot be approximated by atomic-mix homogenization. Even approximations for stochastic-media problems, such as the Levermore-Pomraning (LP) closure[(2,3)] and chord-length sampling[(4)] may include frequent material transitions. These transitions truncate multiple-scattering steps/substeps and pose a special problem for Class I condensed-history (CH) algorithms,[(5)] like the ETRAN model employed by the Integrated Tiger Series (ITS) codes.[(6)] Material boundaries may also pose problems for condensed-transport (CT) Generalized Boltzmann-Fokker-Planck (GBFP) algorithms.[(7,8)] A better understanding of these algorithms is required for electron-transport analysis in stochastic media.

We have implemented new analog and GBFP electron transport methods in the ITS codes. These have limited capabilities, as they do not yet include all energy-loss straggling effects. That is, these methods use the continuous-slowing down (CSD) approximation for electron impact ionization and electronic excitation events. The condensed history method does not have such limitations, and a number of improvements to the CH algorithm have been made to better simulate transport in stochastic media.

In this paper we evaluate material-boundary crossings in several ways. We use both uniformly distributed and randomly distributed material boundaries. The randomly distributed boundaries are implemented as a model for the Levermore-Pomraning (LP) closure in simulating stochastic materials with Markovian material mixing. In this case, the distance to a material boundary is determined by sampling from an exponential distribution based on mean chord length through each material type.[(4)] In many of our test problems we impose material boundaries in a problem composed of only a single material to more easily observe the effects of inducing boundary-crossing artifacts from the algorithms.

The remainder of the paper is organized as follows. In Section II, we discuss the physics and models that are employed in each of the methods examined. In Section III, we briefly discuss stochastic media. We describe the LP-closure approximation that we use, and describe the relevance of our studies here to other stochastic-media simulation methods that might be used. In Section IV, we describe algorithmic improvements that have been made. We also present results to demonstrate the various algorithmic defects and improvements, as well as compare the different methods. We offer some concluding remarks in Section V.

II. Physics and Models

For the calculations presented in this paper, only electron transport is considered. While production of photon radiation due to bremsstrahlung interactions and ionization relaxation are implemented in analog, CT, and CH, these mechanisms are deactivated in all of the results shown. The electron energy loss due to production of bremsstrahlung radiation can be modeled explicitly to capture straggling effects or can be modeled as

CSD. Production of knock-on electrons above the cutoff energy due to electron impact ionization is included in all transport methods, but the energy imparted to these secondary electrons is not correlated with energy loss in the primary electrons. In the analog and CT algorithms, electron impact ionization contributes only to CSD energy loss. In the CH algorithm, the Seltzer-corrected Landau-Blunck-Leisegang energy-loss straggling method[9] is used. As will be shown, we have now included an improvement to the energy-loss straggling logic similar to improvements made in MCNP by Hughes.[10]

In general, all three algorithms are using the same physical data. Some details specific to each algorithm, including the angular scattering models, are described in the following subsections.

1. Analog

In addition to being limited to CSD for electron impact ionization, the analog transport capability is currently limited to using a screened Rutherford model for elastic angular scattering. The locations of electron interactions are randomly sampled based on exponentially distributed distances to interactions. CSD is enforced between interaction sites. For simplicity, the CSD is currently implemented using a piecewise constant model of the mean energy loss based on integration of the stopping power between energy grid values (the same stopping power data employed in the CH algorithm). The type of interaction is randomly sampled in proportion to the respective cross sections of each possible interaction type. Each interaction is processed before continuing to the next interaction.

2. Condensed Transport

In past work we have explored CT algorithms for electron transport (which we have called GBFP methods). These include random sampling of the distance to angular deflections and energy losses,[7,8] while employing a lower total interaction cross section than analog electron scattering. Implementation of this method requires no special treatment at a material boundary. We use a method by Sloan[11] and Morel[12] to generate discrete scattering angles. In the results presented here, we employ a simple hybrid model: the screened Rutherford distribution is sampled for large angular deflections ($-1.0 \le \mu \le \mu_{cut}$) and a single discrete scattering angle is used for small angular deflections ($\mu_{cut} \le \mu \le 1.0$). Unless otherwise stated, the cutoff angle between these two models is $\mu_{cut} = 0.9$.

3. Condensed History

In contrast to the analog and CT methods, interactions are not always processed sequentially. For example, after an electron has been moved a substep, the locations of bremsstrahlung interactions are determined processed. If multiple bremsstrahlung events occurred in a given substep, their locations are randomly sampled and are processed in the order sampled, which is not necessarily sequentially along the electron path. Energy loss due these bremsstrahlung interactions is only deducted in the order sampled during processing of bremsstrahlung events and only from the electron at the end of the substep. That is, energy loss due to bremsstrahlung events does not affect the sampling of knock-on production during the substep.

ITS uses Goudsmit-Saunderson CH angular-scattering distributions.[5] These exactly describe the angular direction-of-flight for particles that have traversed a prescribed pathlength, if the energy is not changing or the angular-scattering cross section is not changing with energy. We refer to this prescribed pathlength as a "substep." Another multiple-scattering approximation determines the energy-loss treatment over a "step". In addition to approximately accounting for changes in energy of the electron over the substeps within a step, the spatial displacement of the electron must be approximated. ITS uses a simple efficient model: sampled energy-loss is applied continuously over the step, sampled angular-deflection is applied at the end of each substep, an approximate angular deflection is sampled for truncated substeps, and the energy treatment is reset for a truncated step. The frequent truncation of steps and substeps due to material-boundary crossings in stochastic media invokes approximations, which need to be better characterized.

III. Stochastic Media

While the improvements in the boundary crossing algorithm apply to any problem, they are especially necessary for simulaton of stochastic media. Stochastic media problems arise when the mean chord lengths through materials are larger than the transport mean free path, such that material homogenization cannot be used, but small enough that geometry realizations cannot be efficiently analyzed. One of the oldest and simplest approximations for simulating stochastic media is the Levermore-Pomraning (LP) closure.[2] In a Monte Carlo algorithm, the closure requires that the distance to a material interface is randomly sampled from an exponential distribution. The closure is a Markovian approximation, so the distance to an interface is resampled any time the particle scatters, and the history of boundary crossings is not remembered during the transport. That is, a backscattered particle will see different material interface locations. While more accurate algorithmic closures have been devised for Monte Carlo codes, in which interfaces or portions of the geometry can be remembered, we only evaluate the LP closure here. No matter how the stochastic media is generated, the electron boundary-crossing algorithms will affect the accuracy of the transport.

IV. Numerical Results

Many of the test problems in this section use only a single-material slab. Boundary crossings are artifically introduced to trigger the boundary-crossing approximations and assess their accuracy. For example, when the LP algorithm is used, unless otherwise stated, both materials in the stochastic mixture are the same and the algorithm is merely sampling the locations at which the boundary-crossing logic is employed. It should be noted that the error of these boundary crossings was recognized long ago, and the code avoids the boundary-crossing logic when adjacent zones are composed of identical material. For testing purposes, it was necessary to circumvent this logic.

All calculations were performed with only electron transport. Angular scattering always used the screened Rutherford model, to permit consistency between the existing methods. Angular deflection of the primary electron due to impact ionization was neglected.

1. No Angular Scattering and No Energy-Loss Straggling

Even in the continuous-slowing down (CSD) logic, boundary-crossing artefacts were introduced. The energy-loss over an electron step was determined by the energy at the start of the step using a nearest-neighbor algorithm to determine the mean-energy loss to be applied. Since boundary crossings initiate a new step, some straggling in the CSD energy loss could be introduced based on the outcomes of the nearest-neighbor data at the boundary crossings. Because an electron always completed a step, unless a boundary was encountered, it continued to lose energy even if it fell below the cutoff energy. This resulted in discrepancies in the energy at which particles were stopped below cutoff. These artifacts were initially detected when tally subzones were smaller than an electron step, and it was observed that a material boundary caused the electron cutoff enforcement to deposit a disproportionate number of electrons in subzones adjacent to the artificial material boundary.

We investigated these artifacts by examining charge deposition from 30 keV electrons normally incident on silicon. Angular scattering and energy-loss straggling were deactivated. Electron deposition as a function of the electron range is shown in Fig. 1. Both the analog and condensed history (CH) results initially differed from the expected result. Calculations were performed in a pure material with the analog ("Analog") and condensed history ("CH") algorithms, and also with both algorithms while imposing artificial material boundaries based on the LP algorithm ("Analog LP" and "CH LP").

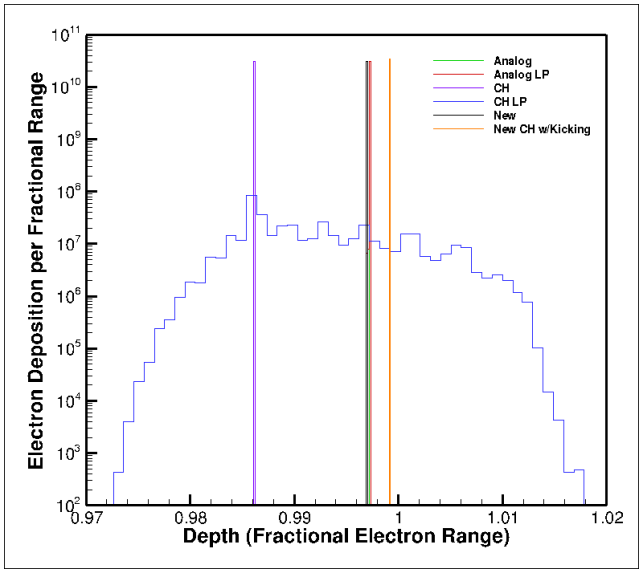

Figure 1: Charge deposition distributions from various algorithms with continuous-slowing down and no angular scattering.

Two modifications were required in the algorithm to achieve consistent results. It was necessary to halt electrons at energy boundaries in the mean energy-loss data and begin new "steps" with updated data. It was necessary to consistently halt electrons when they reach the cutoff energy. The variation was much greater in the CH results, because they were subject to both of these corrections. The analog algorithm as initially implemented did not halt electrons at the cutoff energy. Because the condensed history algorithm always completed a step, the range of the electron was sensitive to the initial alignment of the energy of the electron with the energy grid of the mean energy-loss data.

As an aside, the CH algorithm has an additional feature not yet implemented in the analog or CT methods. "Kicking" is a below-cutoff correction that moves an electron a fraction of the remaining electron range. Kicking is based on the "practical" range of the electron. The practical ranges are empirically determined values which capture the expected range of the electron while accounting for angular scattering and energy-loss straggling. The ratio of the practical range to the CSD range of a 30 keV electron in silicon is 0.725. That is consistent with the fractional range that the condensed history results with kicking differ from the new condensed history results without kicking and 1.0. That is, the electrons reaching cutoff are being kicked 72.5% of their remaining range. Kicking is omitted in all subsequent results in this paper.

2. Angular Scattering

We have investigated the boundary-crossing algorithms associated with angular scattering using a test problem of 30 keV electrons normally incident on silicon. In the following studies straggling due the production of bremsstrahlung radiation was enabled, but all other energy loss was modeled as CSD. The energy deposition profile is shown in Fig. 2 for the default analog, CH, and GBFP algorithms (without artificial material boundaries).

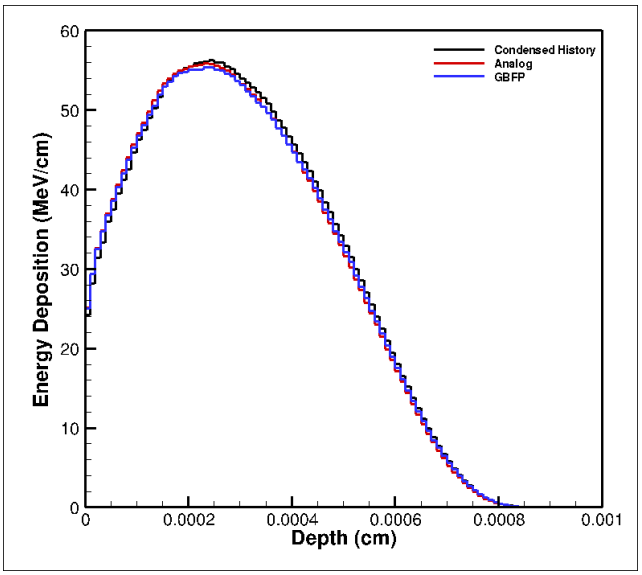

Figure 2: Energy deposition distributions from the analog, condensed history, and GBFP algorithms with angular scattering and continuous-slowing down.

In Fig. 3 we show the results from the CH algorithm (as a

ratio to the analog results) for calculations performed with decreasing substep sizes. As would be hoped, decreasing the substep size improves the agreement between the CH and analog results. In fact, the only statistically significant error remaining in the most refined cases is at the front edge of the slab. The CH method is always somewhat in error at this location because it requires that the electron complete one substep before any angular deflection is sampled.

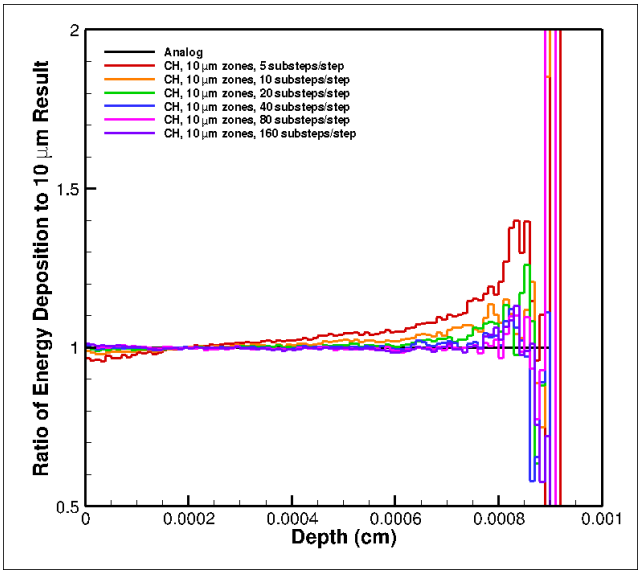

Figure 3: Convergence of condensed history to analog results with decreasing substep size.

In the previous section we found that we achieved improvements by halting electron steps at energy grid values where the mean energy-loss data changed. In Fig. 3 we perfomred the CH substep-size study while halting electron steps and truncating electron substeps at these energy grid values. The excellent agreement here suggests that the approximate angular scattering due to truncating substeps for changes in the stopping power is an insignificant effect. The analog invokes no approximation for the changes in stopping power, but the condensed history converges to good agreement with it. This is compared to the existing algorithm in ITS which always continues with the step even if the electron energy has fallen to a lower energy due to a large energy-loss event. A similar substep-size study without truncation of substeps at energy boundaries or halting the electron step is shown in Fig. 4. Comparison with Fig. 3 suggests that truncation of substeps and halting electron steps to allow for the change in angular scattering and mean energy-loss data improves the accuracy of the CH algorithm.

In Fig. 5 we perform the same study of decreasing substep size in the CH method, with artificial material boundaries included every 100 nm through the thickness of the slab. The inclusion of material boundaries greatly increases the error in condensed history results. Decreasing the substep size reduces this error. This is because a greater number of substeps are being taken without encountering a material boundary. However, the CH results do not appear to be converging to the analog results.

We found two improvements necessary in the boundary-crossing logic for angular scattering: Electrons must be allowed

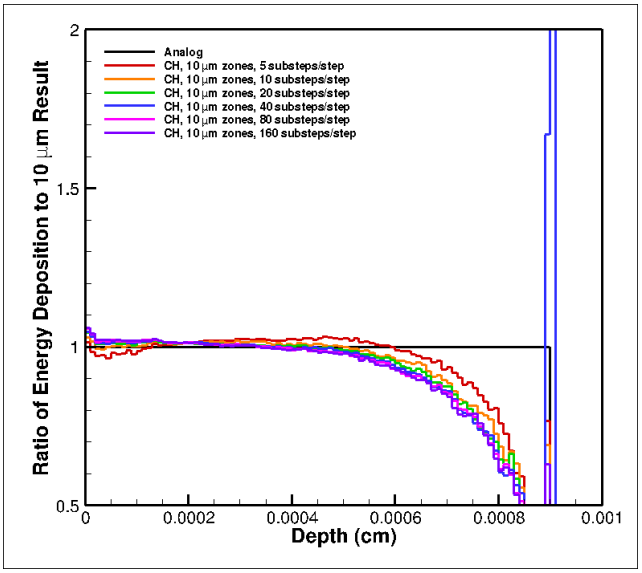

Figure 4: Convergence of condensed history to analog results with decreasing substep size, without substep truncation at energy boundaries in the energy-loss data.

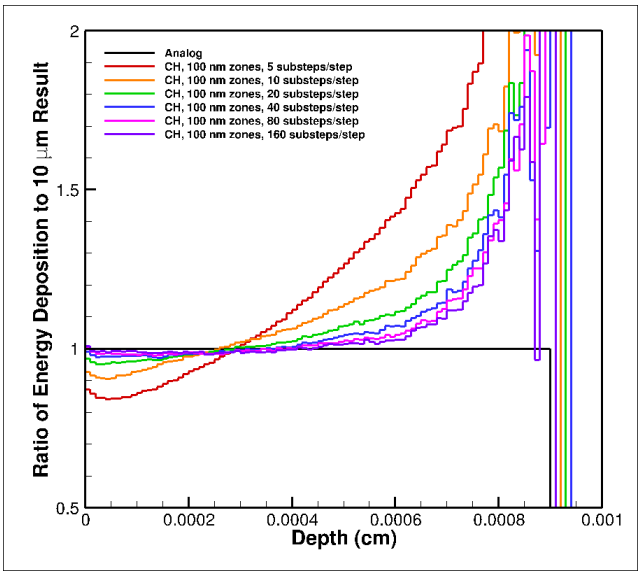

Figure 5: Convergence of condensed history to analog results with decreasing substep size in the presence of many material boundaries.

to backscatter even when a material boundary is encountered, and electrons cannot be moved away from material boundaries inconsistent with the transport mechanics of the problem.

The CH algorithm used in ITS samples angular deflection at the end of the electron substep. When the substep is truncated due to encountering a material boundary, the angular deflection is sampled at the material boundary using the approximate Jordan-Mack algorithm.[13] The existing ITS algorithm rejects any angular deflection that would cause the electron to not cross the material boundary and resamples the angular dflection until an acceptable electron direction is found. While simplifying the electron tracking logic, this introduces errors that become significant when many material boundaries are encountered. We have implemented logic in ITS that permits electrons to backscatter even when a material bounary is encountered.

The same substep-size study was performed while allowing electrons to backscatter at material boundaries. The results are shown in Fig. 6. These results show significant deviation from the analog results especially near the end of the electron range. Further, the results do not appear change appreciably with decreasing substep size. This indicates that the convergence seen in the previous results when backscatter is forbidden at boundaries is only due to the increase in backscatter that is allowed as the substep size is decreased and a greater number of substeps complete without encountering a material boundary.

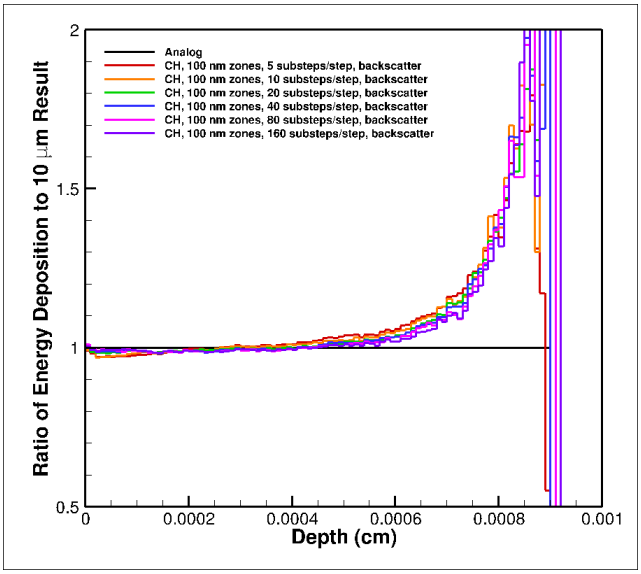

Figure 6: Convergence of condensed history to analog results with decreasing substep size in the presence of many material boundaries while permitting backscatter at boundaries and including the 1 nm boundary-push feature.

Finally, we demonstrate the effect of one additional modification made to the original algorithm. ITS pushes electrons that have crossed a material boundary by an extra nanometer into the next zone. This is done with no associated track tally or energy loss to the electron. (This features has been deemed necessary in the three-dimensional code to improve the robustness of geometry interrogation. However, there do not appear to have been reasons to include this logic in the one-dimensional code.) The same substep-convergence study was performed with the boundary-push logic, and the results are shown in Fig. 7. These results start very close to the analog results and appear to converge with decreasing substep size. By comparison with Fig. 6, the failure of the previous results to converge to the analog solution is entirely attributable to the boundary-push feature. This problem using low energy electrons and 100 nm zones is especially vulnerable to this feature.

It is especially interesting to compare Fig. 7 with Fig. 3. We note that even though numerous boundaries have been included, the results with a low number of substeps per step are actually more accurate than the comparable results without material boundaries. Even though an approximate angular distribution is being employed at the boundary crossings, the increase in the number of simulated substeps (both truncated and non-truncated) due to boundary crossings makes the simulation more accurate.

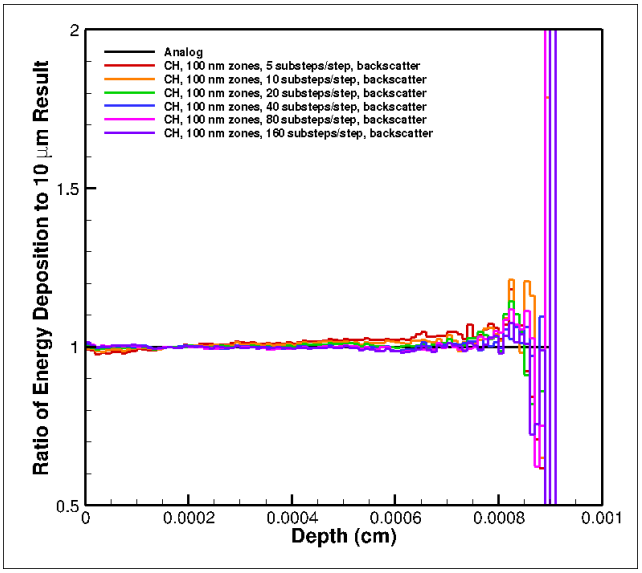

Figure 7: Convergence of condensed history to analog results with decreasing substep size in the presence of many material boundaries while permitting backscatter at boundaries.

To demonstrate the effectiveness of these improvements in the CH method for stochastic media simulations, we compare analog and CH results in Fig. 8. Three materials are simulated with equal portions of nitrogen and silicon: a homogenized mixture, finely mixed material with mean chord lengths of 1 μm, and a coarsely mixed material with mean chord lengths of 10 μm. We have not performed a substep-size study, but in light of the previous results, the descrepancies appear to be primarily due to substep-size artifacts.

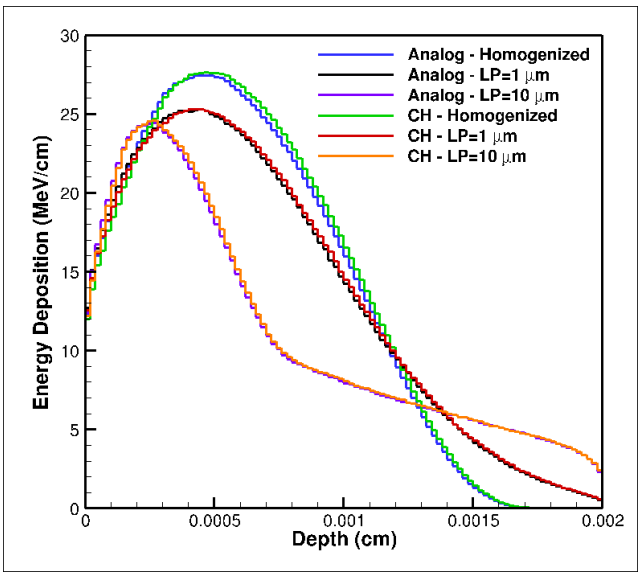

Figure 8: Energy deposition distributions comparing analog and condensed history algorithms with angular scattering and continuous-slowing down in homogenized and Levermore-Pomraning material mixes.

For comparison, the analog results for the problems are compared with GBFP results in Fig. 9. The GBFP results appear to be in somewhat better agreement with the analog results than were the CH results.

We have also examined reflection of electrons using a 1 MeV

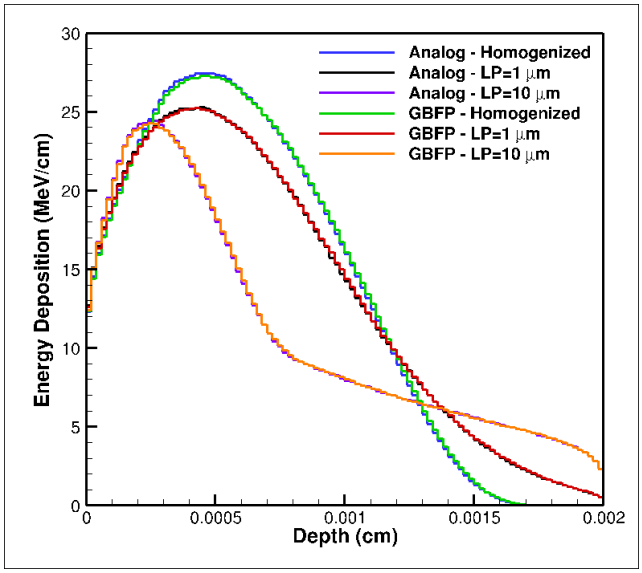

Figure 9: Energy deposition distributions comparing analog and GBFP algorithms with angular scattering and continuous-slowing down in homogenized and Levermore-Pomraning material mixes.

source of electrons normally incident of silicon. The reflection spectrum is especially difficult for the ITS condensed history algorithm, because it requires on substep to be taken before an electron can backscatter. The analog results and default CH results are shown in Fig. 10.

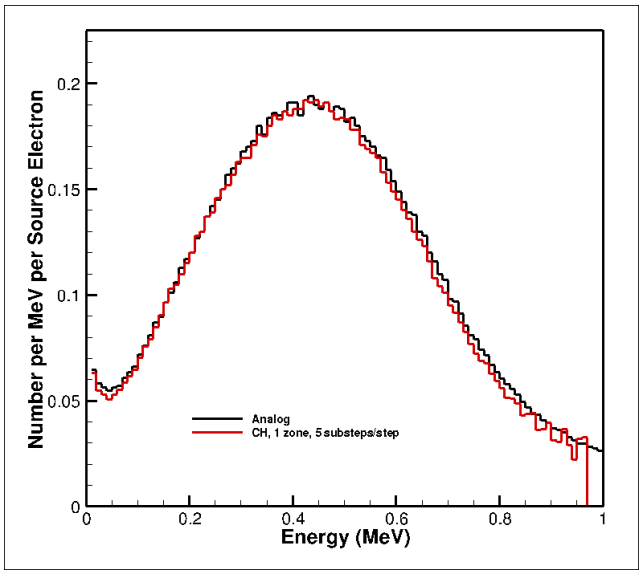

Figure 10: Energy spectrum of reflected electrons for 1 MeV electrons normally incident on silicon.

In Fig. 11 we show the reflection-spectrum results from a substep-size study with condensed history results provided as a ratio to the analog results. These simulations all used a 0.25 cm slab (thicker than the range of a 1 MeV electron in silicon) modeled as a single zone. The CH results do not appear to be converging to the analog results.

Substep-size studies were also performed with material boundaries placed every 25 μm. The results forbidding and permitting backscatter at material boundaries are shown in Figs. 12 and 13. The existing algorithm performs quite poorly with the

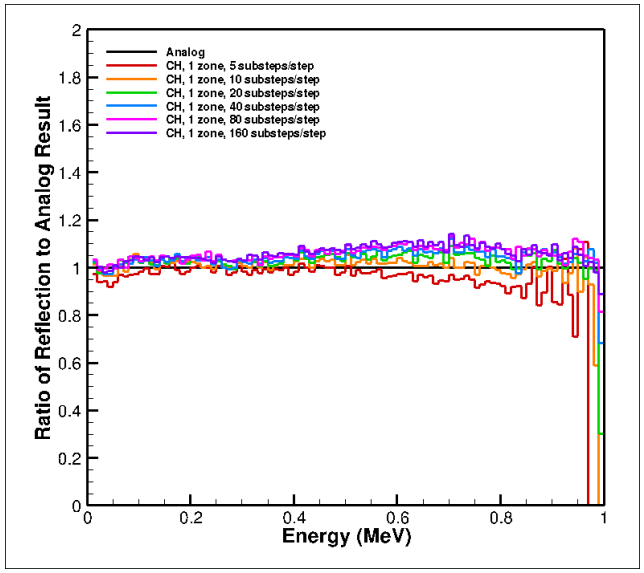

Figure 11: Condensed history results with decreasing substep size compared to analog for the energy spectrum of reflected electrons.

default substep size, because the suppression of backscatter in the algorithm especially degrades the accuracy for this calculation. When backscatter at boundaries is permitted the accuracy appears to be comparable to the algorithm in the absence of material boundaries. All of the CH algorithms appear to be converging to comparable results that are not in statistical agreement with the analog results. At the higher energy of this problem, this could be due to stability issues in the recursion relations used to generated the CH angular-scattering distributions. This issue has previously been studied[14] and should be revisited for this problem. It is also possible that differences in the angular treatment between the CH and analog implementation are causing these discrepancies.

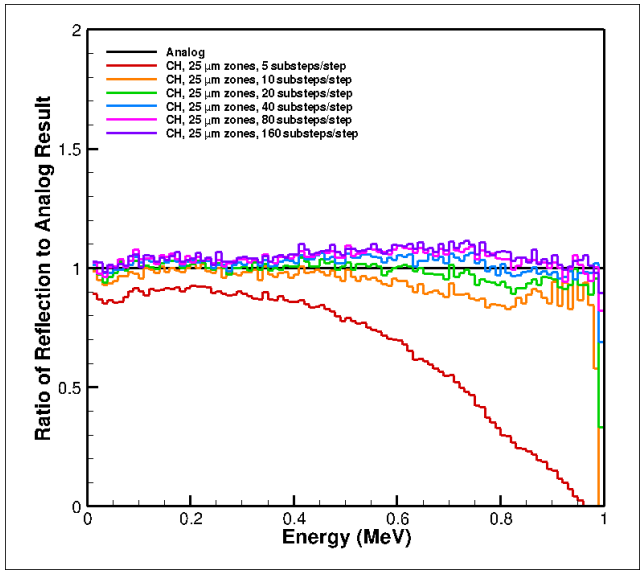

Figure 12: Condensed history results with decreasing substep size compared to analog for the energy spectrum of reflected electrons. Artificial material boundaries are included at 25 μm intervals in depth.

Next we evaluate the GBFP algorithm. For the same prob-

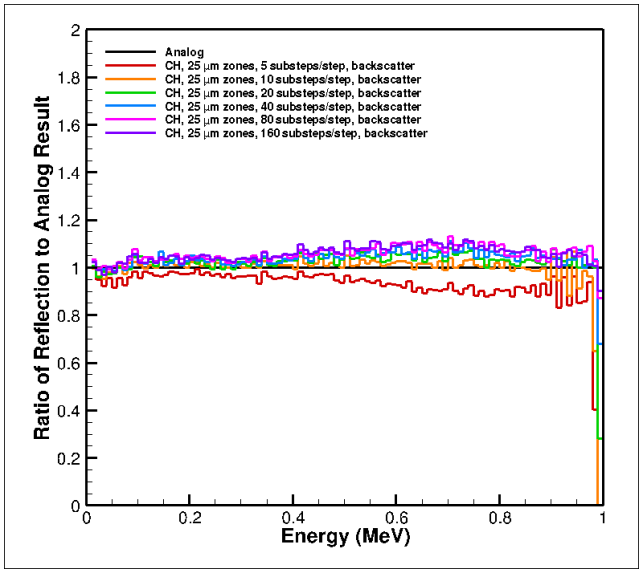

Figure 13: Condensed history results with decreasing substep size compared to analog for the energy spectrum of reflected electrons. Artificial material boundaries are included at 25 μm intervals in depth.

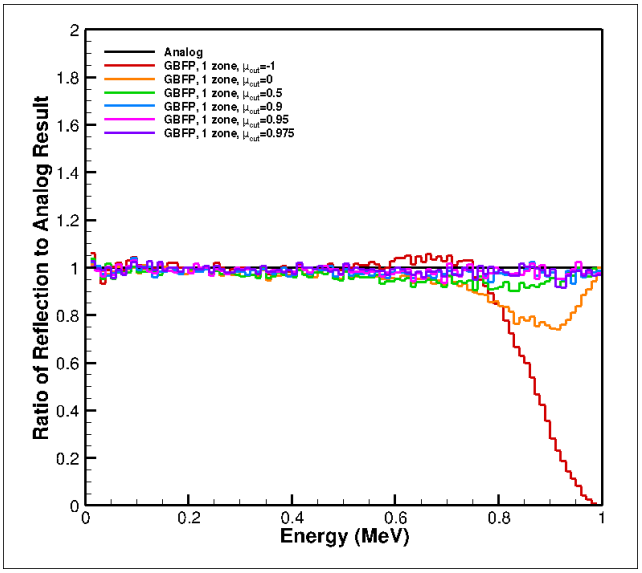

Figure 14: Convergence of GBFP to analog results with increasing μ_{cut}.

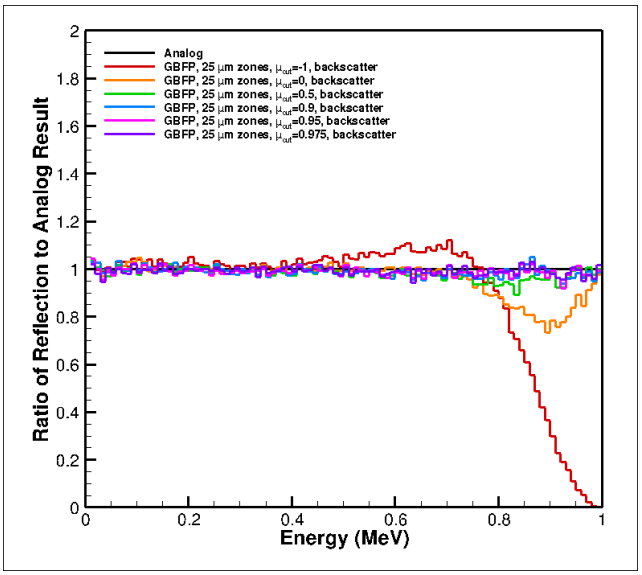

Figure 15: Convergence of GBFP to analog results with increasing μ_{cut} in the presence of many material boundaries.

lem of 1 MeV electrons normally incident on a silicon slab, we performed a series of calculations while varying the μ_{cut} that separates the hard collisions which are sampled from the screened Rutherford distribution and the soft collisions that are approximated by a single discrete scattering angle. The results in the absence and presence of material boundaries are shown in Figs. 14 and 15. Not surprisingly, modeling all of the angular scattering with a single discrete angle is inaccurate, especially in underpredicting the reflection of high-energy electrons. A $\mu_{cut} \geq 0.9$ produces results that are generally in statistical agreement with the analog results for this problem. The GBFP reflection in the highest energy bin exceeds the analog result by a statistically significant ratio in all except the $\mu_{cut} = -1$ case. This may be due to a discrepancy in the treatment of the angular scattering, where the screening parameter in the analog simulation is interpolated to the energy of the electron interacting, whereas the discrete scattering angles are employed using a nearest-neighbor algorithm.

3. Energy-Loss Straggling

Hughes[10] had shown an improvement in the energy-loss sampling algorithm in MCNP. We have reproduced his results in ITS, showing both the same problem he had documented and showing improvements through similar modifications to the algorithm. We studied the same problem: the transmission energy spectrum of electron due to 10 MeV electrons normally incident on 15 mm of water. Angular scattering and the production of secondary electrons are both deactivated. We include energy-loss straggling due to the production of bremsstrahlung photons, but no photons are produced in the simulations. All simulations use a fundamentally identical problem description, and division into smaller zones introduces artificial material boundaries. These artificial boundaries trigger the boundary crossing approximations.

Results are shown in Fig. 16 based on the existing ITS algorithm. The sizes of the zones in the problem geometry dramatically alter the results. The energy-loss straggling is being sampled at the start of an electron step and evenly apportioned across all substeps in the step. When the step is truncated due to a material boundary, a new step is initiated. Thus, the energy loss applied to the electron was based on an incorrect assumption about the distance the electron would be transported and on the coarse assumption of linear energy loss along the path. Not only is the mean energy loss of the electron incorrect, but also the straggling. The energy-loss sampling across an electron step has been carefully tuned to achieve the correct mean energy loss and straggling, but these attributes are lost for a truncated step.

Seltzer[9] devised an approach for scaling the energy-loss sampling to a fractional step. This logic has been used in ITS to adjust the energy of escaping electrons, but has not

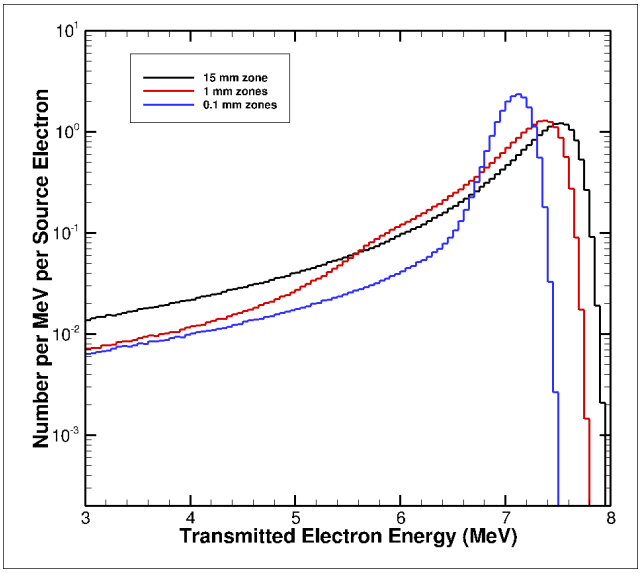

Figure 16: Transmission spectrum through 15 mm of water showing the effects of material boundaries on the energy-loss algorithm.

been used for internal boundary crossings. The existing logic was also based on precomputing many energy-loss sampling parameters on a fixed energy grid. We have now modified ITS to perform energy-loss sampling based on the fractional step (i.e., the substep or truncated substep) that an electron will travel. To a large extent the energy-loss sampling no longer uses precomputed data. (The integrated mean energy loss over a step is the current exception, though this could be replaced by an on-the-fly integration of the stopping power over the expected travel distance.)

Results obtained using the new energy-loss straggling algorithm are shown in Fig. 17. We find that the results with and without artificial material boundaries are in statistical agreement.

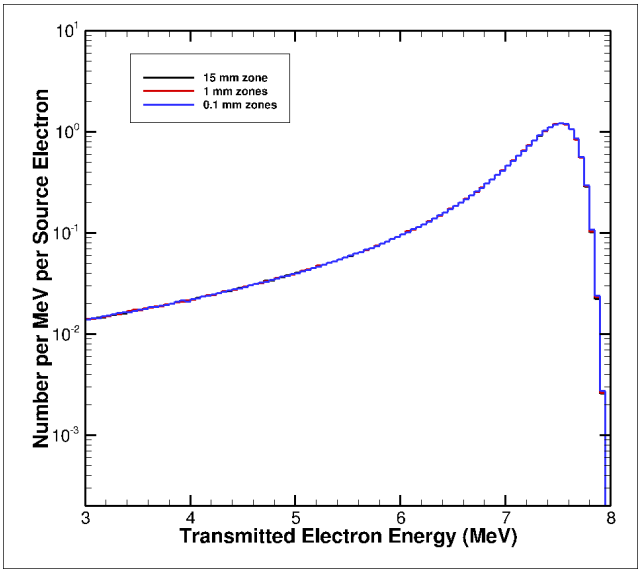

Figure 17: Transmission spectrum through 15 mm of water showing the minimal effects of material boundaries on the new energy-loss algorithm.

The defect in the energy-loss algorithm and the improvement due to the revised algorithm are also observed with the LP algorithm. Transmission results through a single material with artificial boundaries imposed by the LP algorithm are shown in Fig. 18. In these calculations the mean distance to a material boundary was 0.1 mm (the same as distances between boundaries in the finest divisions in the previous test problems). In these calculations, secondary knock-on electrons due to impact ionization events were also tracked and dominate the transmission spectrum below 3.5 MeV.

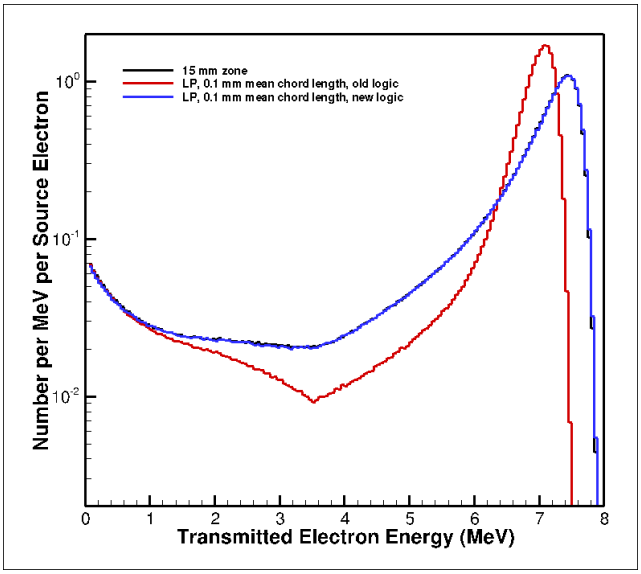

Figure 18: Convergence of condensed history to analog results with decreasing substep size in the presence of many material boundaries while permitting backscatter at boundaries.

V. Conclusions

We have assessed the accuracy of the electron transport algorithms in the Integrated TIGER Series codes for stochastic-media simulations. These problems are especially sensitive to the boundary-crossing algorithms that are employed. As a result of our investigations, we have implemented numerous improvements in the algorithms. In calculations using the continuous-slowing-down approximation, we have modified the algorithms to (1) consistently employ the precalculated mean energy-loss data and (2) consistently enforce the energy cutoff. In calculations using angular scattering, we have modified the condensed history algorithm to (1) truncate substeps at energy boundaries in the mean energy-loss and other data, (2) permit backscatter from the angular-deflection sampling due to truncated substeps at material boundaries, (3) and eliminate artificial particle movements across material boundaries. In calculations with energy-loss straggling, we have implemented a pathlength-based straggling algorithm. Where possible, we have compared the improvements in the condensed history algorithm against analog simulations. We have also assessed the accuracy of the GBFP condensed transport method against analog simulations and generally found it to be robust in the presence of material interfaces.

Acknowledgments

Thanks to John Jones for performing much of the work in implementing the analog capability in ITS. Sandia National Laboratories is a multi-program laboratory managed and operated by Sandia Corporation, a wholly owned subsidiary of Lockheed Martin Corporation, for the U.S. Department of Energy's National Nuclear Security Administration under contract DE-AC04-94AL85000.

References

1) E. Larsen and L. Liang, "The Atomic Mix Approximation for Charged Particle Transport," *SIAM J. Appl. Math.*, **68**, *1*, 43-58 (2007).
2) M. Adams, E. Larsen, and G. Pomraning, "Benchmark Results for Particle Transport in a Binary Markov Statistical Medium," *J. Quant. Spectrosc. Radiat. Transfer*, **42**, 253-266 (1989).
3) R. Sanchez, "Linear Kinetic Theory in Stochastic Media," *J. Math. Physics*, **30**, 2948-2511 (1989).
4) G. Zimmerman and M. Adams, "Algorithms for Monte-Carlo Particle Transport in Binary Statistical Mixtures," *Trans. Am. Nucl. Soc.*, **64**, 287-288 (1991).
5) in *Monte Carlo Transport of Electrons and Photons*, edited by T. M. Jenkins, W. R. Nelson, and A. Rindi, Plenum Press, New York, 1988.
6) B. Franke, R. Kensek, T. Laub, and M. Crawford, "ITS Version 6: The Integrated TIGER Series of Coupled Electron/Photon Monte Carlo Transport Codes," SAND2008-3331, Sandia National Laboratories (2009).
7) B. Franke and A. Prinja, "Monte Carlo Electron Dose Calculations Using Discrete Scattering Angles and Discrete Energy Losses," *Nucl. Sci. Eng.*, **149**, 1-22 (2005).
8) B. Franke, A. Prinja, and L. Harding, "Monte Carlo Electron Transport Using Generalized Boltzmann Fokker-Planck Scattering Models," *Proc. Mathematics and Computation, Supercomputing, Reactor Physics, and Nuclear and Biological Applications*, Palais des Papes, Avignon, France, September 12–15, 2005.
9) S. Seltzer, "Electron-Photon Monte Carlo Calculations: The ETRAN Code," *Appl. Radiat. Isot.*, **42**, *10*, 917-941 (1991).
10) H. Hughes, "Improved Logic for Sampling Landau Straggling in MCNP5," *Proc. Mathematics and Computation, Supercomputing, Reactor Physics, and Nuclear and Biological Applications*, Palais des Papes, Avignon, France, September 12–15, 2005.
11) D. P. Sloan, "A New Multigroup Monte Carlo Scattering Algorithm Suitable for Neutral and Charged-Particle Boltzmann and Fokker-Planck Calculations," SAND83-7094, Sandia National Laboratories (1983).
12) J. E. Morel, L. J. Lorence, R. P. Kensek, J. A. Halbleib, and D. P. Sloan, "A Hybrid Multigroup/Continuous-Energy Monte Carlo Method for Solving the Boltzmann-Fokker-Planck Equation," *Nuclear Science and Engineering*, **124**, 369-389 (1996).
13) D. Jensen, "Monte Carlo Calculation of Electron Multiple Scattering in Thin Foils," Master's thesis, Naval Postgraduate School, Monterey, CA, 1988.
14) R. Keith and R. Kensek, "Order-of-Convergence Study of a Condensed-History Algorithm Implementation," *Proc. International Conference on Mathematics, Computational Methods & Reactor Physics (M&C 2009)*, Saratoga Springs, New York, May 3–7, 2009.